HEP'99 # 7_573
Submitted to Pa 7
Pl 7, 8

DELPHI 99-96 CONF 283
15 June 1999

Search for R-parity violation with a $\bar{U}\bar{D}\bar{D}$ coupling at $\sqrt{s} = 189$ GeV

Preliminary

DELPHI Collaboration

Paper submitted to the HEP'99 Conference
Tampere, Finland, July 15-21

Search for R-parity violation with a $\bar{U}\bar{D}\bar{D}$ coupling at $\sqrt{s} = 189$ GeV

R. Barbier [1], P. Jonsson [1], S. Katsanevas [1]
[1]IPN, Lyon (France)

Abstract

Searches for pair production of gauginos and squarks in e^+e^- collisions at a centre-of-mass energy of 189 GeV have been performed on data corresponding to an integrated luminosity of 158 pb^{-1} collected by the DELPHI detector at LEP. The data were analyzed under the assumption of non-conservation of R-parity through a single dominant $\bar{U}\bar{D}\bar{D}$ coupling between squarks and standard quarks. Typical final states contain between 4 and 10 jets with or without additional leptons. No excess of data above Standard Model expectations was observed. The results were used to constrain domains of the MSSM parameter space and derive limits on the masses of supersymmetric particles.

The following mass limits were obtained from these searches:

- Lightest Neutralino mass limit : $m_{\tilde{\chi}_1^0} \geq 30$ GeV
- Lightest Chargino mass limit : $m_{\tilde{\chi}_1^+} \geq 94$ GeV
- Stop and Sbottom mass limit (indirect decay) :
  - $m_{\tilde{t_1}} \geq 70.5$ GeV, for $\Phi_{mix} = 0$ rad
  - $m_{\tilde{t_1}} \geq 52.5$ GeV, for $\Phi_{mix} = 0.98$ rad
  - $m_{\tilde{b_1}} \geq 66.5$ GeV, for $\Phi_{mix} = 0$ rad

1 Introduction

1.1 The R-parity violating Lagrangian

The most general way to write a superpotential including the symmetries and particle content of the Minimal Supersymmetric extension of the Standard Model (MSSM) [1] is:

$$W = W_{MSSM} + W_{RPV} \tag{1}$$

where W_{MSSM} represents interactions between MSSM particles consistent with $B - L$ conservation (B = baryon number, L = lepton number) and W_{RPV} describes interactions violating B or L conservation [2]. These latter terms of the superpotential can explicitly be written as[1] [3]:

$$\lambda_{ijk} L_i L_j \bar{E}_k + \lambda'_{ijk} L_i Q_j \bar{D}_k + \lambda''_{ijk} \bar{U}_i \bar{D}_j \bar{D}_k \tag{2}$$

where i, j and k are the generation indices; L and $\bar{E}$ denote the left-handed doublet lepton and the right-handed singlet charge-conjugated lepton superfields respectively, whereas Q, $\bar{U}$ and $\bar{D}$ denote the left-handed doublet quark and the right-handed singlet charge-conjugated up- and down-type quark superfields; λ_{ijk}, λ'_{ijk} and λ''_{ijk} are the Yukawa couplings. The first two terms violate L conservation, and the third one B conservation. Since $\lambda_{ijk} = -\lambda_{jik}$, $\lambda''_{ijk} = -\lambda''_{ikj}$, there are 9 λ_{ijk}, 27 λ'_{ijk} and 9 λ''_{ijk} leading to 45 additional couplings.

One major phenomenological consequence of $\not{R}_p$ is that the Lightest Supersymmetric Particle (LSP) is allowed to decay into standard fermions. This fact modifies the signatures of the supersymmetric particle production compared to the expected signatures in case of R-parity conservation. In this paper, searches for pair produced neutralinos ($\widetilde{\chi}_i^0$), charginos ($\widetilde{\chi}^{\pm}$) and squarks ($\widetilde{q}$) were performed under the hypothesis of R-parity violation with one single dominant $\bar{U}\bar{D}\bar{D}$ coupling. The $\bar{U}\bar{D}\bar{D}$ terms couple squarks to quarks and the experimental signature of the $\not{R}_p$ events thus becomes multiple hadronic jets, and in most of the cases without missing energy.

1.2 Pair production of gauginos and sfermions

Pair production of supersymmetric particles with $\not{R}_p$ is the same as R_p conserved pair production since the $\bar{U}\bar{D}\bar{D}$ couplings do not enter in the production vertex.

The mass spectrum of neutralinos and charginos is fixed in the analyses described in this paper by the three parameters of the MSSM theory assuming GUT scale unification of gaugino masses : M_2, the SU(2) gaugino mass parameter at the electroweak scale, μ, the mixing mass term of the Higgs doublets at the electroweak scale and $tan\beta$, the ratio of the vacuum expectation values of the two Higgs doublets.

The pair production of squarks ($\tilde{q}$) is also studied in this paper. Here the cross section mainly depends on the squark masses. In the case of the third generation, the left-right mixing angle enters in the production cross section as well. In the squark analysis two cases are considered : one with no mixing, the second with the mixing angle which gives the lowest production cross section.

[1] An additional fourth term in eq.2, describing a bilinear coupling between the left handed lepton superfield and the up-type Higgs field, is assumed to be zero.

1.3 Direct and indirect decays of gauginos and sfermions

The decay of the produced sparticles can be either direct or indirect. In a *direct decay* the sparticle decays directly or via a virtual sparticle exchange to standard particles through an $\not{R}_p$ vertex. In an *indirect decay* the sparticle first decays through an R_p conserving vertex to a standard particle and an on-shell sparticle, which then decays through an $\not{R}_p$ vertex. The squark analysis is done considering only the indirect decay channels which are dominant for coupling values considered in the present studies.

Table 1 shows the various possible direct and indirect decays of supersymmetric particles via $\bar{U}\bar{D}\bar{D}$ couplings.

Direct decay	$\widetilde{q}\rightarrow q_1\ q_2 \quad \widetilde{\chi}_1^0\rightarrow q_1\ \widetilde{q^*}\rightarrow q_1\ q_2q_3 \quad \widetilde{\chi}^{\pm}\rightarrow q_1\ \widetilde{q^*}\rightarrow q_1\ q_2q_3$
Indirect decay	$\widetilde{\chi}^{\pm}\rightarrow W^{*+}\ \widetilde{\chi}_1^0\rightarrow q_1q_2\ q_3q_4q_5$ or $l^+\nu\ q_3q_4q_5 \quad \widetilde{q}\rightarrow q_1\ \widetilde{\chi}_1^0\rightarrow q_1\ q_2q_3q_4$

Table 1: Neutralino, chargino and squark decays when one $\bar{U}\bar{D}\bar{D}$ coupling is dominant.

The most important features of these decays are the number of quarks in the final state which goes up to 5 for the indirect chargino decay. Table 2 displays the different event topologies from direct and indirect decays through $\bar{U}\bar{D}\bar{D}$ couplings of different pair produced sparticles.

final states	direct decay of	indirect decay of
$4j$	$\widetilde{q}\widetilde{q}$	
$6j$	$\widetilde{\chi}_1^0\widetilde{\chi}_1^0$, $\widetilde{\chi}_2^0\widetilde{\chi}_1^0$, $\widetilde{\chi}_1^+\widetilde{\chi}_1^-$	
$8j$		$\widetilde{\chi}_2^0\widetilde{\chi}_1^0$, $\widetilde{q}\widetilde{q}$
$10j$		$\widetilde{\chi}_1^+\widetilde{\chi}_1^-$

Table 2: The multijet final states in neutralino, chargino and squark pair production when one $\bar{U}\bar{D}\bar{D}$ coupling is dominant.

1.4 $\bar{U}\bar{D}\bar{D}$ Couplings

The $\bar{U}\bar{D}\bar{D}$ Yukawa coupling strength, corresponding to a squark decay into two quarks, can be bound from above (indirect limits) and below (sensitivity of this analysis).

Upper limits on $\bar{U}\bar{D}\bar{D}$ couplings come from Standard Model constraints with experimental measurements:

- heavy nucleon decays for λ''_{112} couplings [4],
- $n-\bar{n}$ oscillations for λ''_{113} [5],
- $R_l = \Gamma_{had}(Z^0)/\Gamma_l(Z^0)$ for $\lambda''_{312}, \lambda''_{313}, \lambda''_{323}$ [6, 7].

The upper limits on the other λ'' couplings do not come from experimental bounds. They are obtained from the requirement of perturbative unification at the GUT scale of

10^{16} GeV. This gives a limit of 1.25 for a sfermion mass of 100 GeV [8, 4]. Upper limits on the $\bar{U}\bar{D}\bar{D}$ couplings are reported in table 3 [9].

ijk	$\lambda''_{ijk} \leq$	ijk	$\lambda''_{ijk} \leq$	ijk	$\lambda''_{ijk} \leq$
$\lambda''_{uds}(112)$	10^{-6}	$\lambda''_{cds}(212)$	1.25	$\lambda''_{tds}(312)$	0.43
$\lambda''_{udb}(113)$	10^{-5}	$\lambda''_{cdb}(213)$	1.25	$\lambda''_{tdb}(313)$	0.43
$\lambda''_{usb}(123)$	1.25	$\lambda''_{csb}(223)$	1.25	$\lambda''_{tsb}(323)$	0.43

Table 3: Limits [9] on the $\bar{U}\bar{D}\bar{D}$ Yukawa couplings in units of $(m_{\tilde{f}}/100$ GeV), where $m_{\tilde{f}}$ is the appropriate squark mass.

Our analysis, which does not search for long lived sparticles in the detector (displaced vertices), has a limited sensitivity to weak coupling strengths. Therefore, a limit can be imposed by requiring a short mean decay length L which is given by [10, 11]:

$$L(\mathrm{cm}) = 0.1\ (\beta\gamma) \left(\frac{\mathrm{m_{\tilde{f}}}}{100\ \mathrm{GeV}}\right)^4 \left(\frac{1\ \mathrm{GeV}}{\mathrm{m_{\widetilde{\chi}}}}\right)^5 \frac{1}{\lambda''^2} \tag{3}$$

if the neutralino or the chargino is the LSP or by

$$L(\mathrm{cm}) = 10^{-12}\ (\beta\gamma) \left(\frac{1\ \mathrm{GeV}}{\mathrm{m_{\widetilde{f}}}}\right) \frac{1}{3\lambda''^2} \tag{4}$$

if the sfermion is the LSP. In the two previous formulae $\beta\gamma = P_{\widetilde{\chi},\widetilde{f}}/m_{\widetilde{\chi},\widetilde{f}}$. Our typical lower limit of sensitivity for this analysis ($L \lesssim 1$ cm) is of the order of 10^{-4} (10^{-3}) in case of a $\widetilde{\chi}^0$or a $\widetilde{\chi}^{\pm}$ of 30 GeV (10 GeV), with a squark mass of 100 GeV, and 10^{-7} in case of sfermions.

Note that in these analyses the λ''_{212} coupling value was set to 0.1 for signal generation and for the MSSM interpretation of the results. No assumption on the quark flavour has been made. Searches for decays via λ'' couplings leading to the production of one or several b quarks, have the advantage of using b-tagging techniques and have better sensitivity. Therefore, we can safely assume that the results obtained for the λ''_{212} are valid for the 8 other λ''_{ijk} couplings too.

2 Data and MC samples

The analysis was performed on the data corresponding to an integrated luminosity of 158 pb^{-1} collected during 1998 by the DELPHI detector [12] at centre-of-mass energies around 189 GeV.

Concerning the background, the different contributions coming from the Standard Model processes: four fermion final states (WW, ZZ, $qqee$, $qq\mu\mu$ and $qq\tau\tau$) and Z$\gamma\rightarrow$ $q\bar{q}(\gamma)$ were considered. The contribution from $\gamma\gamma$ events after preselection was found to be negligible, due to the high detected energy fraction and multiplicities of the studied signals. For the Z$\gamma\rightarrow$ $q\bar{q}\gamma$ backgrounds, the PYTHIA [13] generator was used whereas the four fermion final states were generated with EXCALIBUR [14].

To evaluate signal efficiencies, sparticle production was generated using SUSYGEN [15]. All generated signal events were processed with the DELPHI detector simulation program (DELSIM).

3 Analyses

3.1 Topologies and analysis strategy

The present study covers the search for $\widetilde{\chi}_1^0$, $\widetilde{\chi}_1^+$and $\widetilde{q}$ pair production. The analysis of the different decay channels can be organized on the basis of the number of hadronic jets in the final state.

For each multijet analysis, the clustering of hadronic jets was performed by the *ckern* package[16] based on the Cambridge clustering algorithm[17]. The choice of this clustering algorithm was motivated by its good performance for configurations with a mixture of soft and hard jets, the expected case for $\bar{U}\bar{D}\bar{D}$ events. Moreover, the algorithm provides a good resolution for the jet substructure which is present in $\bar{U}\bar{D}\bar{D}$ indirect decays. For each event, *ckern* provides all possible configurations between two and ten jets. The values of the variables $y_{(i+1)i}$, that is the transition value of the DURHAM resolution variable y_{cut}, which change the characterization of an event from an i to an $i+1$ jet configuration, constitute a powerful tool to identify the topologies in multijet signals. Note that the $y_{(i+1)i}$ flip value in the following will be called $y_{(i+1)}$.

A neural network method was applied in order to distinguish signals from Standard Model background events. The SNNS [18] package was used for the design and training of the neural networks. The training was done on samples of simulated background and signal. The exact configuration and input variables of each neural network depended on the search channel. Each neural network provided a discriminant variable which was used to select the final number of candidate events for each analysis.

3.2 Hadronic preselection

A first preselection of pure hadronic events was performed at the starting point of all analyses reported below.

The following preselection criteria were applied :

- the charged multiplicity had to be greater or equal to 15;
- the total energy from charged particles was required to be greater than $0.30 \times \sqrt{s}$,
- the total energy was required to be greater than $0.55 \times \sqrt{s}$,
- the total energy from neutral particles was required to be less than $0.50 \times \sqrt{s}$.

With this preselection most of the $\gamma\gamma$ background was suppressed. Tighter requirements on charged multiplicity included in each analysis made this background negligible. Note that the radiative return on the Z peak was suppressed by the effective centre-of-mass energy and the most energetic photon criteria. Therefore in what follows the main background events will be the four fermion events like $W^+W^-$and the $Z\gamma$ QCD events with hard gluon radiation. Signal efficiency at the level of hadronic preselection was between 80% and 90% for high and medium mass of pair produced sparticles. The preselection efficiency for the lowest neutralino mass was around 70 %. After the hadronic preselection the agreement between the number of observed events (4722) in data and the number of expected events (4736) from SM processes was rather good. Figure 1 shows the distributions of several variables after this hadronic preselection.

3.3 Charginos and neutralinos, 6 and 10 jet analyses

The 6 jet analysis was divided into 3 mass windows to take into account the magnitude of the neutralino boost depending on its mass:

- Window N1; low neutralino mass: $10 \leq m_{\tilde{\chi}} \leq 30$ GeV.
- Window N2; medium neutralino mass: $30 < m_{\tilde{\chi}} \leq 70$ GeV.
- Window N3, high neutralino mass: $70 < m_{\tilde{\chi}} \leq 94$ GeV.

The 10 jet analysis was more sensitive to the mass difference between the chargino and the neutralino than to the neutralino mass. To take into account this mass difference we divided the 10 jet analysis in 2 windows:

- Window C1; low chargino neutralino mass difference i.e. $\Delta M \leq 10$ GeV.
- Window C2; high chargino neutralino mass difference i.e. $\Delta M > 10$ GeV.

The signal selection in both channels was performed in two steps. First, we applied soft sequential criteria against mainly $Z\gamma$ QCD events except in the case of the low neutralino mass window.

- the effective centre-of-mass energy had to be greater than 150 GeV,
- the energy of the most energetic photon had to be less than 30 GeV,
- the sphericity had to be greater than 0.05, the thrust lower than 0.92 and it was required -log(y_3) lower than 6.

Second, a neural network method was used to select the signal against the four fermion background. For each window analysis a specific neural network has been trained. Topological variables used as inputs to the network are listed in what follows :

- oblateness,
- -log(y_n) with n=4 to 10,
- minimum di-jet mass in 4, 5 and 6 jet configurations,
- energy of the less energetic jet $\times$ minimum di-jet angle in 4 and 5 jet configurations.

The training was performed in a standard back-propagation manner using the SNNS package [18]. The network configuration was 13 input nodes, 13 hidden nodes and 3 output nodes. The 3 output nodes correspond to the signal, the $Z\gamma$ background and the four fermion background. This choice was motivated by the fact that we were looking for different signal topologies which were either similar to $Z\gamma$ or to four fermion events depending on the analysis window.

3.3.1 Direct decay of $\widetilde{\chi}_1^0\widetilde{\chi}_1^0$ or $\widetilde{\chi}_1^+\widetilde{\chi}_1^-$ in 6 jets

Working point optimization on the neural network output was performed minimizing the expected exclusion limit as a function of the signal efficiency. The neural network output of the medium neutralino mass analysis is given in figure 2.

The working points of the neural network output were 0.953, 0.852 and 0.966 for mass windows N1, N2 and N3 respectively. The corresponding signal efficiencies were around 10-15%, 25-30% and 20-30% for the mass windows N1, N2 and N3 respectively. To obtained signal effcencies, the full detector simulation has been performed on neutralino pair production with a 10 GeV step grid in neutralino mass (10 to 94 GeV).

Figure 3 represents the expected and obtained number of events in data as a function of the signal efficiency for the N2 window analysis. No excess of data over background has been observed for each mass window analysis. First, we obtained 13 events in data with 11.5 expected events ($Z\gamma$) for the low neutralino mass window. Second, we obtained 25 events in data with 23.8 expected events ($Z\gamma$ and W^+W^-) for the medium neutralino mass window. Third, we obtained 8 events in data with 6.3 expected events (W^+W^-) for the high neutralino mass window.

3.3.2 Indirect decay of $\widetilde{\chi}_1^+$ $\widetilde{\chi}_1^-$ in 10 jets

The same method was applied to select 10 jet events coming from indirect chargino decays.

Two neural networks for the two different windows were produced. The optimal working points have been found with the same procedure as for the 6 jet analysis. The neural network output values were 0.894 and 0.956 for two mass difference windows (C1 and C2). The corresponding signal efficiencies were around 15-25% and 35-50% for the two mass difference windows. Figure 5 represents the number of expected events and data events as a function of the signal efficiency for the C2 window analysis.

No excess was found in observed events compared to expected background in each analysis window. After the selection procedure 28 events remained in the data compared to the expected 25.7 events for the low mass difference window analysis. For the large mass difference window analysis, 18 events remained in the data compared to the expected 21.1 events.

3.4 Squark analysis

Searches for squarks were performed in the case of indirect decays through a dominant R-parity violating $\bar{U}\bar{D}\bar{D}$ coupling. The general analysis methods based on a neural network background rejection were adopted for the analysis. The search was performed for a generic $\bar{U}\bar{D}\bar{D}$ coupling with no consideration taken to flavour dependent properties, e.g. b-tagging. The simulated decay actually used for the studies and efficiency evaluation was $\widetilde{b}\rightarrow b\ \widetilde{\chi}_1^0$. The final states in the indirect decay channel contain eight quarks of any flavour, but the topology of the signal strongly depends on the mass of the $\widetilde{\chi}_1^0$, through which the decay proceeds. SUSY signals were therefore simulated at different squark masses in the range 50-90 GeV with $\widetilde{\chi}_1^0$ masses between 10-80 GeV.

The analysis was aimed at a good sensitivity for R-parity violating $\bar{U}\bar{D}\bar{D}$ signals all over the plane of kinematically available squark and $\widetilde{\chi}_1^0$ masses. First a general preselection, additional to the one presented in section 3.2, was made with the aim of

a high general efficiency for the signal and at the same time a good rejection of low multiplicity hadronic background events. The preselection criteria were the following:

- the total energy from neutral particles had to be less than $0.47 \times \sqrt{s}$,
- the total event energy had to be greater than $0.53 \times \sqrt{s}$
- the total number of charged particles had to be greater than 20,
- the energy of the most energetic photon in the event had to be less than 45 GeV,
- the missing momentum of the event had to be less than 76 GeV,
- the oblateness of the event had to be less than 0.5.

A neural network was thereafter trained to calculate a discriminant variable for each event, in order to distinguish a possible signal from standard model backgrounds. The following quantities were used as input to the neural network:

- the total energy from neutral particles, the total event energy, the total number of charged particles, the energy of the most energetic photon in the event, the missing momentum of the event, the oblateness of the event,
- -log(y_n) with $n = 2$ to 10,
- the reconstructed mass from a 5 constraints kinematical fit performed on the 4 jet topology of the event and the χ^2 value of this fit,
- the minimum angle between two jets times the minimum jet energy from the 5 jet topology of the event.

Note that some of the input variables for the neural network were also used for the preselection, i.e. the preselection was used to eliminate the signalfree regions and thereby unnecessary background from the analysis, whereas the neural network served to discriminate the signal from the background, in the remaining regions with overlapping values of the variables. The final selection of candidate events was made based on the output value of the neural network. No excess of data over Standard Model backgrounds was observed. After the signal selection, 22 events remained in the data compared to the expected 18.4 events.

The signal efficiency was evaluated at each of the 30 evenly distributed simulated points in the plane of squark and neutralino masses and interpolated in the regions between. Efficiencies for the signal after the final selection range from 10-20%, for small or large mass differences between squark and neutralino, up to 50% for medium mass differences.

4 MSSM interpretation of the results

No excess was seen in the data with respect to the expected background in any of the channels of these analyses. Therefore, limits at 95 % confidence level on the cross section of each process can be obtained. Mass limits can then be derived for supersymmetric particles.

4.1 Chargino and neutralino multijet searches

The experimental cross section (σ_{95}) that can be excluded at 95 % confidence level, is obtained from data and SM event numbers obtained at the end of each analysis. Signal efficiency for any value of $\widetilde{\chi}_1^0$ and $\widetilde{\chi}^{\pm}$ masses is interpolated using an efficiency grid determined with signal samples produced with the full Delphi detector simulation. For typical values of tanβ and m_0, a (μ,M_2) point is excluded at 95 % confidence level if the signal cross section times the efficiency at this point is greater than the experimental cross section (σ_{95}).

Adding the 6 jet analysis (used for the direct decay of $\tilde{\chi}_1^+\tilde{\chi}_1^-$ or $\tilde{\chi}_1^0\tilde{\chi}_1^0$) and the 10 jet analysis (used for indirect decay of $\tilde{\chi}_1^+\tilde{\chi}_1^-$) results, an exclusion contour in the μ, M_2 plane at 95 % confidence level has been derived for different values of m_0 (90 and 300 GeV) and tanβ (1.5 and 30). These exclusion contours in the μ, M_2 plane are shown in figure 7. In the exclusion plots the main contribution comes from the study of the chargino indirect decays with the 10 jet analysis, due to the high cross section. The 6 jet analysis becomes crucial in the exclusion plot for low tan β value, low m_0 values and negative μ values. The chargino is mainly excluded up to the kinematical limit. With $m_0 = 500$ GeV and $tan\beta = 1$ we obtained the following lower limits:

- neutralino mass: $m_{\tilde{\chi}_1^0} \geq 30$ GeV,
- chargino mass: $m_{\tilde{\chi}_1^+} \geq 94$ GeV.

Note that this analysis is only sensitive to neutralino masses greater than 10 GeV.

4.2 Indirect squark multijet searches

Exclusion domains are obtained by calculating σ_{95} divided by the signal efficiency for each 1 GeV×1 GeV bin in the neutralino mass versus squark mass plane and comparing to the cross section for pair-produced squarks. The resulting exclusion contours for stop and sbottom squarks can be seen in fig.8. A 100% branching ratio of indirect decays in the neutralino channel was assumed for this exclusion. The performed 8 jet analysis is independent of flavour properties and hence the difference in exclusion between different squarks is only manifested through the magnitude of the production cross section. The exclusion contours from the third generation (stop and sbottom) shown in fig.8 are therefore, more generally, also valid for the other squark generations. By combining the exclusion contours from the squark searches with the constraint on the neutralino mass from the gaugino searches, lower bounds on the squark masses are achieved:

- $m_{\tilde{t_1}} \geq 70.5$ GeV, for $\Phi_{mix} = 0$ rad,
- $m_{\tilde{t_1}} \geq 52.5$ GeV, for $\Phi_{mix} = 0.98$ rad,
- $m_{\tilde{b_1}} \geq 66.5$ GeV, for $\Phi_{mix} = 0$ rad.

Acknowledgements

The financial support of STINT, The Swedish Foundation for International Cooperation in Research and Higher Education, and NFR, The Swedish Natural Science Research Council, is highly appreciated.

References

[1] For reviews, see e.g. H.P. Nilles, *Phys. Rep.***110** (1984) 1; H.E. Haber and G.L. Kane, *Phys. Rep.* **117** (1985) 75.

[2] P. Fayet, *Phys. Lett.* **B69** (1977) 489; G. Farrar and P. Fayet, *Phys. Lett.* **B76** (1978) 575.

[3] S. Weinberg, *Phys. Rev.* **D26** (1982) 287.

[4] J.L. Goity, Marc Sher, Phys. Lett. B 346 (1995) 69, erratum-ibid. B 385 (1996) 500, hep-ph/9412208.

[5] F. Zwirner, Phys. Lett. B 132 (1983) 103.

[6] G. Bhattacharyya, J. Ellis, K. Sridhar, Mod. Phys. Lett. A10 (1995) 1583, hep-ph/9503264; G. Bhattacharyya, D. Choudhury, K. Sridhar, Phys. Lett. B 355 (1995) 193, hep-ph/9504314; J. Ellis, S. Lola, K. Sridhar, e-Print Archive: hep-ph/9705416.

[7] G. Bhattacharyya, Nucl. Phys. Proc. Suppl. 52A (1997) 83, hep-ph/9608415.

[8] B. Brahmachari, Probir Roy, Phys. Rev. D 50 (1994) 39, erratum-ibid. D 51 (1995) 3974, hep-ph/9403350.

[9] H. Dreiner, hep-ph/9707435.

[10] S. Dawson, *Nucl. Phys.* **B261** (1985) 297.

[11] H. Dreiner and G.G. Ross, *Nucl. Phys.* **B365** (1991) 597.

[12] P. Abreu et al., *Nucl. Instr. Meth.* **378** (1996) 57.

[13] T. Sjöstrand, *Computer Phys. Comm.* **39** (1986) 347.

[14] F.A. Berends, R. Kleiss, R. Pittau, *Computer Phys. Comm.* **85** (1995) 437.

[15] S. Katsanevas, P. Morawitz, hep-ph/9711417, sumbitted to Comp. Phys. Comm.

[16] S. Bentvelsen and I. Meyer, hep-ph/9803322, submitted to *Eur. Phys. J.***C**. The *ckern* package can be found on wwcn1.cern.ch/~ stamb/ckern/ckern.html

[17] Yu.L. Dokshitzer, G.D. Leder, S. Moretti, B.R. Webber *J. High Energy Phys.***08** (1997) 001.

[18] A. Zell et al., SNNS User manual, Version 4.1 *Report N 6/95.*

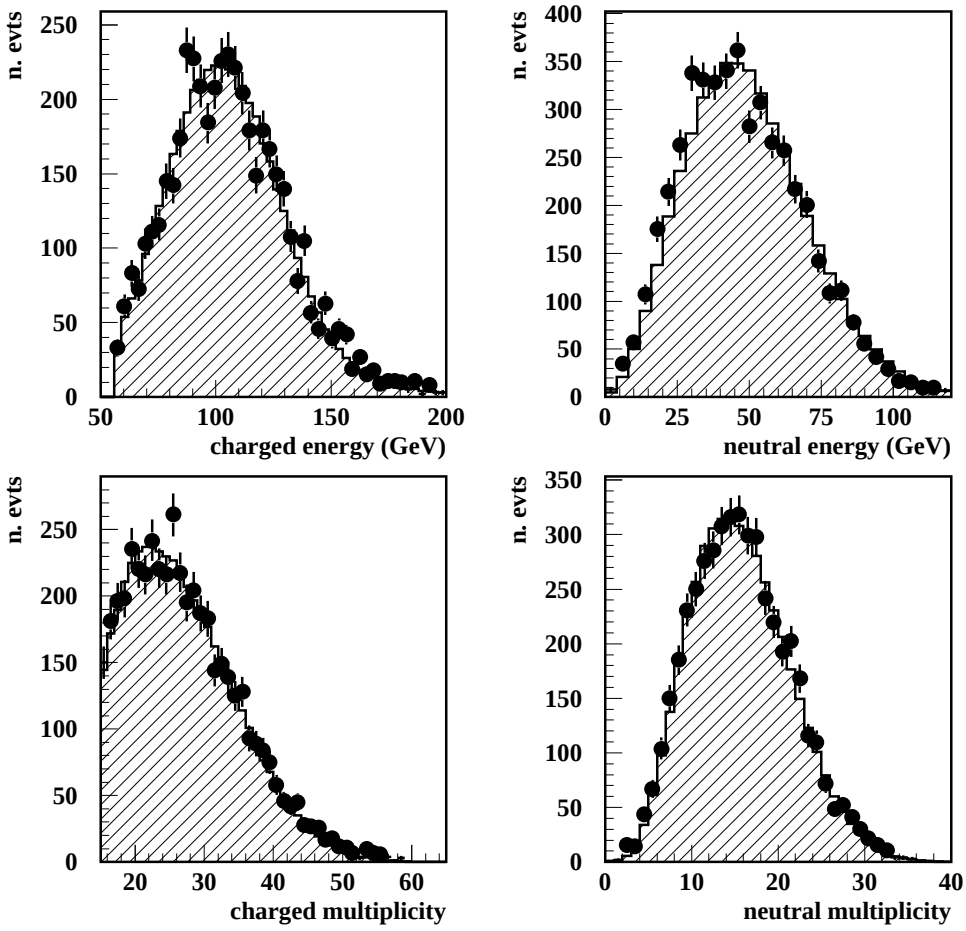

Figure 1: Charged (upper left), neutral (upper right) energy distributions and charged (lower left) and neutral (lower right) multiplicity distributions after hadronic preselection for data (black dots), expected SM background (hatched histograms).

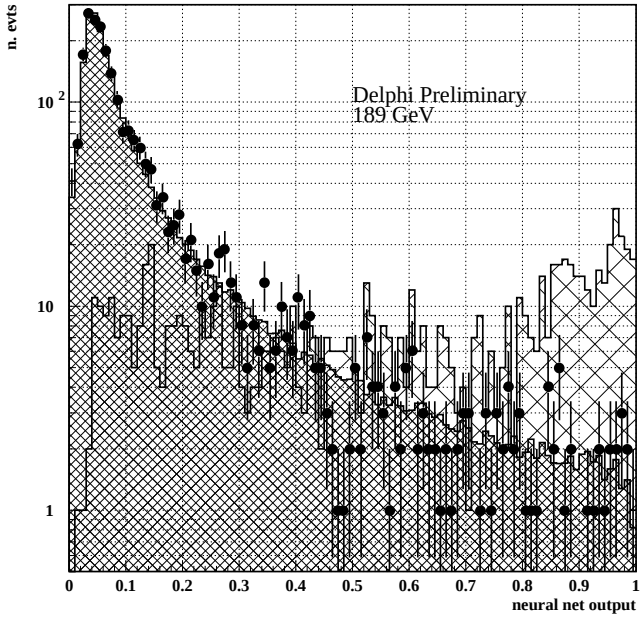

Figure 2: Neural network signal output for data (black dots), expected SM background (tight hatched) and the unweighted signal (loose hatched) for the medium neutralino mass search N2.

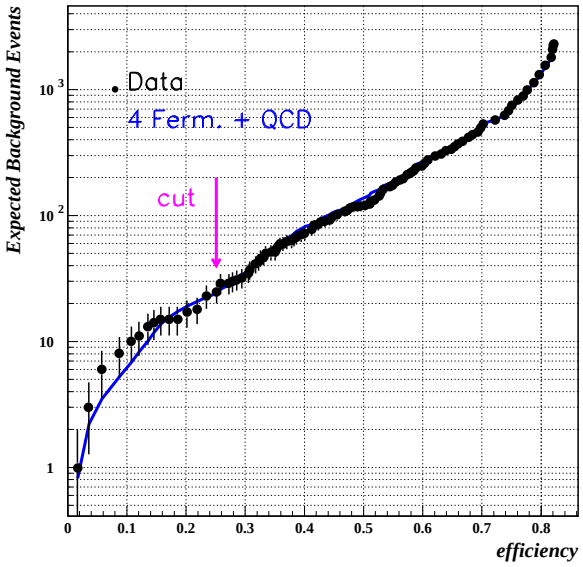

Figure 3: Number of expected events (blue continuous line) data events (black dots) versus signal efficiency for the medium neutralino mass search N2. The arrow shows the efficiency corresponding to the working point.

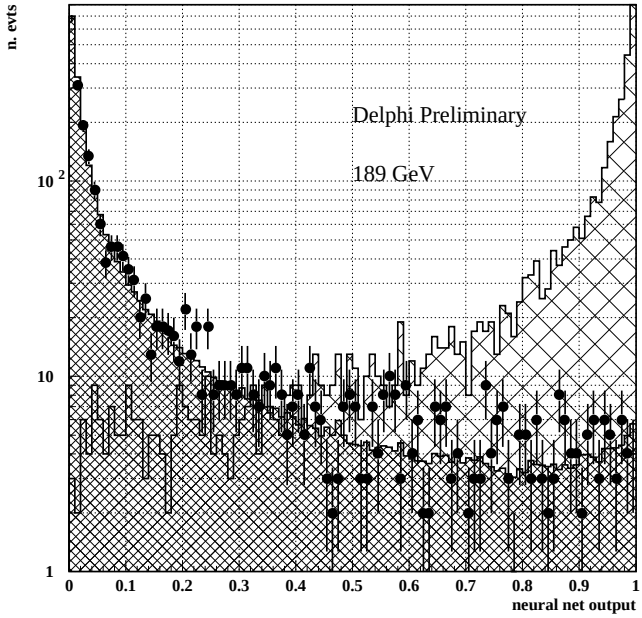

Figure 4: Neural network signal output for data (black dots), expected SM background (tight hatched) and the unweighted signal (loose hatched) for the low ΔM chargino neutralino search C2.

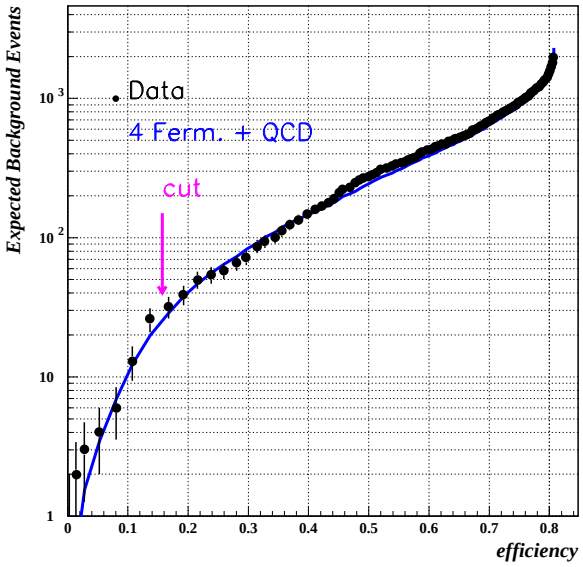

Figure 5: Number of expected events (blue continuous line) data events (black dots) versus signal efficiency for the low ΔM chargino neutralino search C2. The arrow shows the efficiency corresponding to the working point.

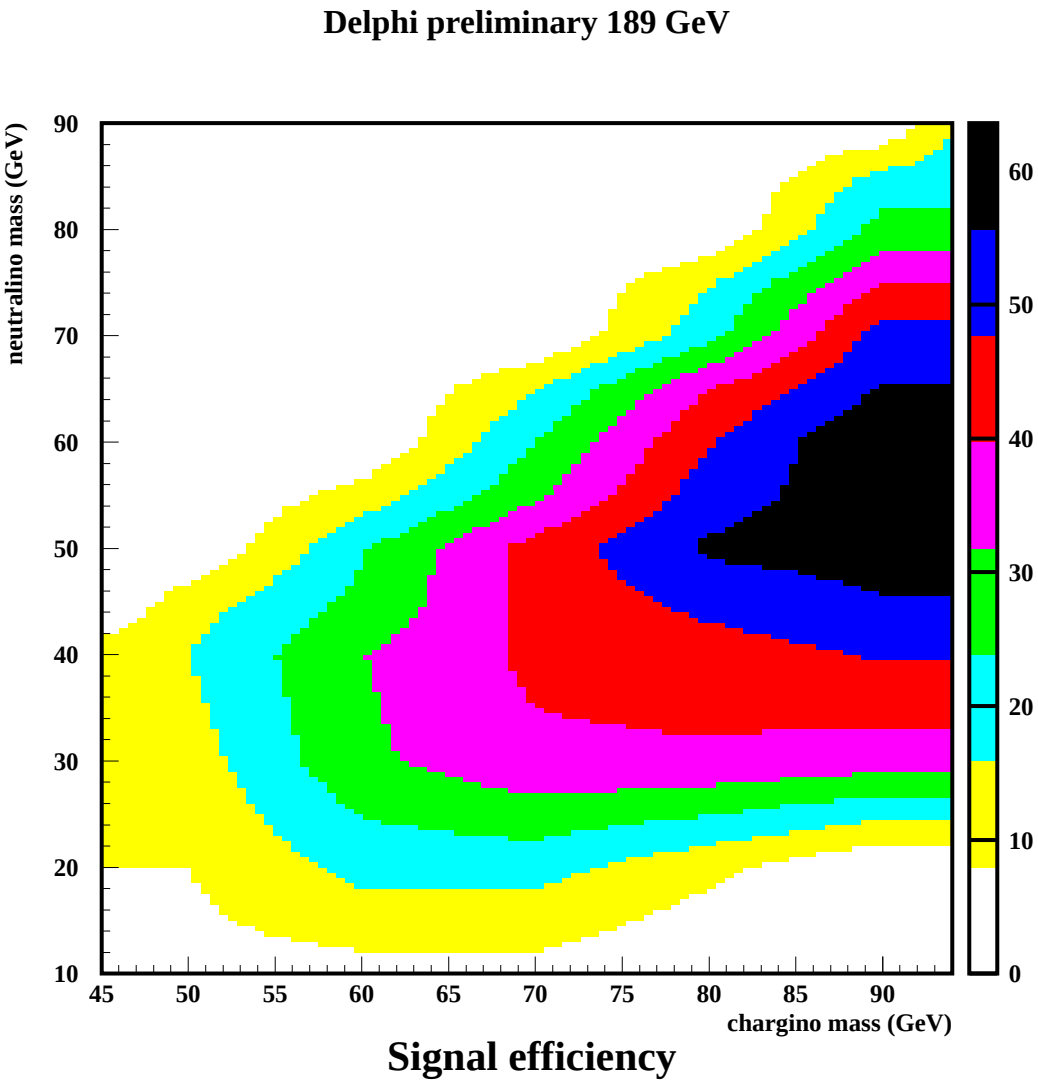

Figure 6: Signal efficiency (%) in chargino versus neutralino mass plane for the 10 jet analysis, corresponding to indirect decay of chargino.

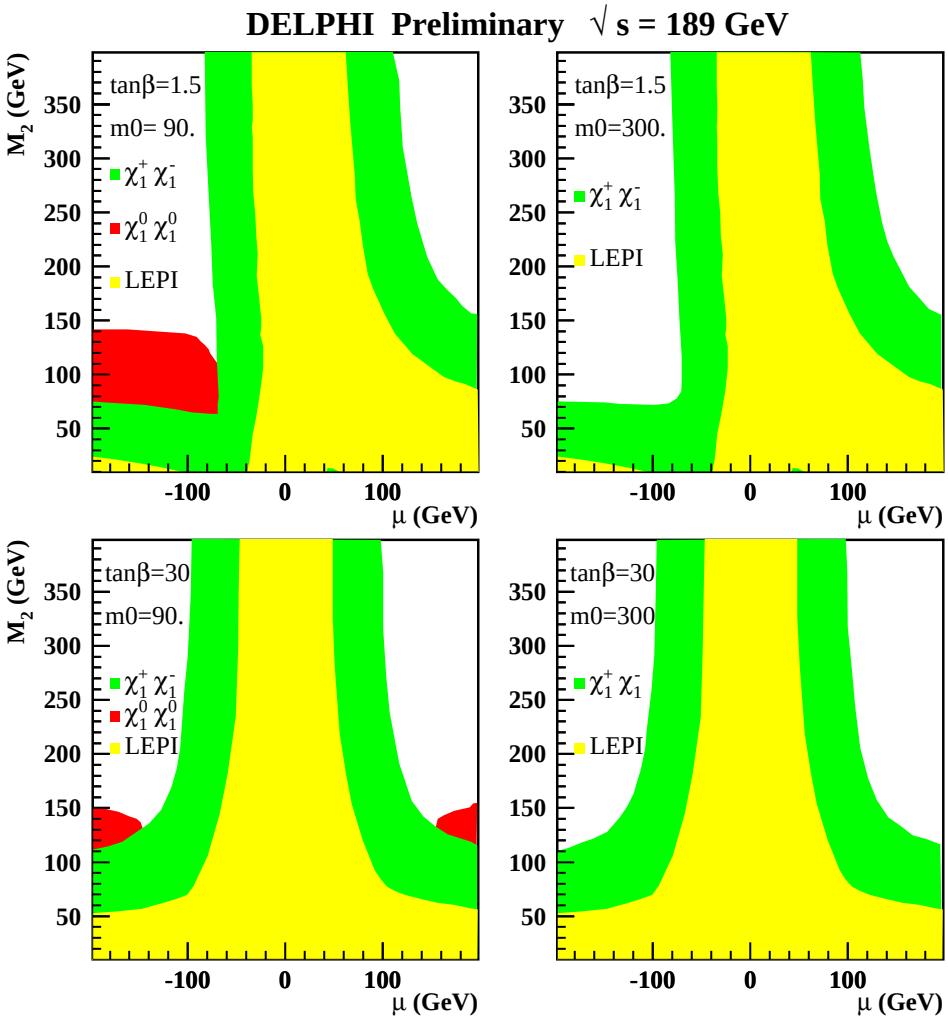

Figure 7: Exclusion plot in μ, M_2 plane for $\tilde{\chi}_1^0\ \tilde{\chi}_1^0$ and $\tilde{\chi}_1^+\ \tilde{\chi}_1^-$ production in the case of a dominant $\bar{U}\bar{D}\bar{D}$ R-parity violation coupling. The 6 and 10 jets analyses are treated separatly for this exclusion.

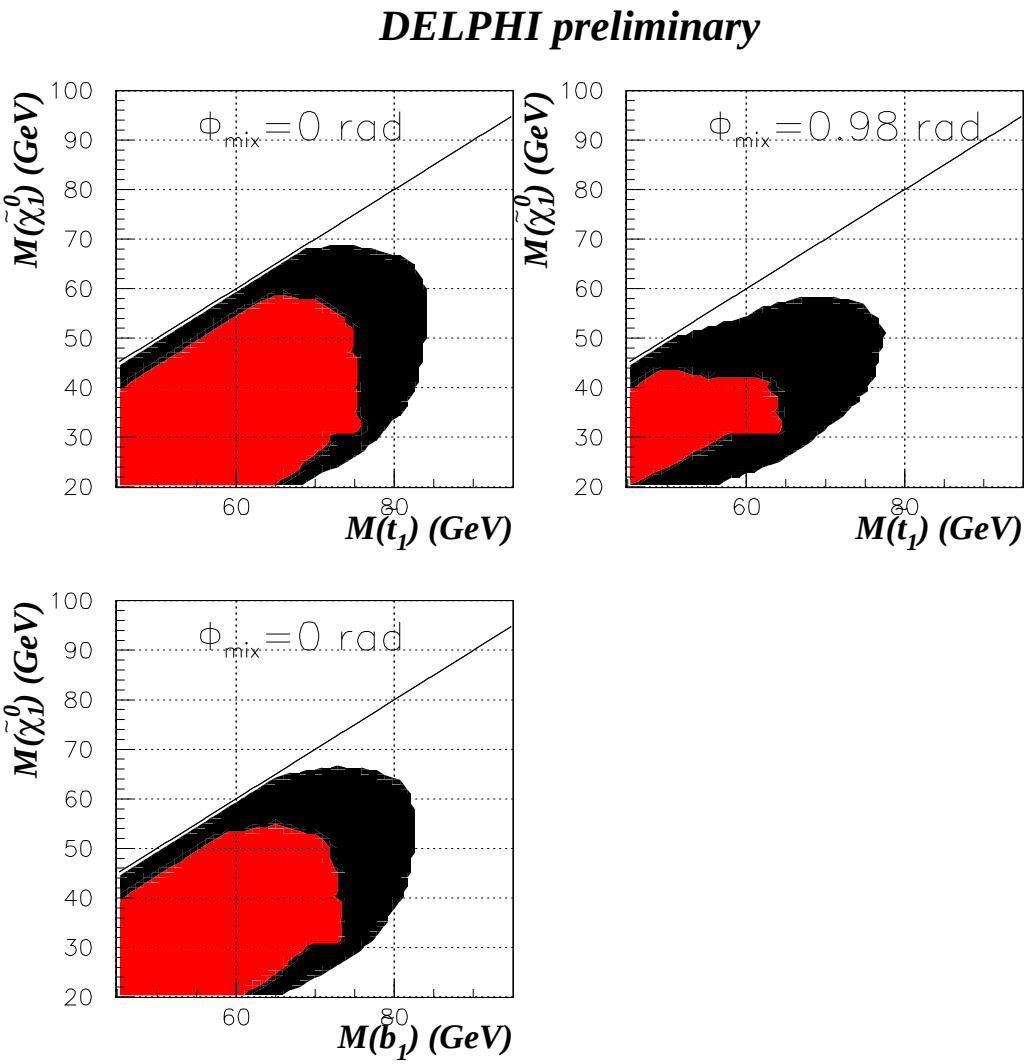

Figure 8: Exclusion domains at 95% confidence level in the $M(\tilde{\chi}_1^0)$, $M(\tilde{q})$ plane for indirect squark decays in the case of a dominant R-parity violating $\bar{U}\bar{D}\bar{D}$ coupling achieved from the analysis of DELPHI data collected at 189 GeV (black). The red colour corresponds to the exclusion domain obtained from the data collected at 183 GeV. The plots to the left show the exclusion for pure left handed stop and sbottom respectively. The upper right plot shows the exclusion for a stop with a minimum cross section producing mixing angle. For sbottom the minimum cross section is too low to extract any exclusion with the present analysis. The diagonal lines indicate the degenerate mass region above which indirect squark decays are kinematically forbidden.